AIP | Journal of Applied Physics

Modeling electron flow produced by a three-dimensional spatially periodic field emitter

A. Rokhlenko and J. L. Lebowitz

Citation: J. Appl. Phys. **108**, 123301 (2010); doi: 10.1063/1.3520672
View online: http://dx.doi.org/10.1063/1.3520672
View Table of Contents: http://jap.aip.org/resource/1/JAPIAU/v108/i12
Published by the American Institute of Physics.

Modeling electron flow produced by a three-dimensional spatially periodic field emitter

A. Rokhlenko[a] and J. L. Lebowitz
Department of Mathematics, Rutgers University Piscataway, New Jersey 08854-8019, USA

(Received 9 August 2010; accepted 27 October 2010; published online 17 December 2010)

We study the space charge limited field emission from an emitter whose surface has a simple periodic structure with bumps. The shape of each bump is represented by a smooth function and the emission is governed by the Fowler–Nordheim–Schottky law. A mathematical scheme for modeling the potential and current structure by a set of elementary functions is developed and implemented numerically with the help of a special least square procedure. Our results show that such emitters are more efficient than emitters with long ridges only in weak electric fields. In stronger fields the latter give larger currents and they should be more durable. The emission by an individual bump in our periodic structure is compared also with that of a single emitter bump of the same shape, they appear to be quite close. © *2010 American Institute of Physics*. [doi:10.1063/1.3520672]

I. INTRODUCTION

The theoretical study of the space charge limited current is a notoriously difficult task. The differential equations describing it cannot be reduced to a standard problem because both the potential and current density are unknown and their mutual dependence is nonlinear. The usual ways of simplification involve assuming the presence a very strong magnetic field, which makes the electron trajectories predetermined, and imposing symmetries which reduce the dimensionality of the problem. While the assumption of a magnetic field can be justified based on theoretical and experimental studies[1] which showed that it does not change very much the final result, this is not so clear for the dimensionality reduction. The two- dimensional (2D) and three-dimensional (3D) spacial structure of the field emitters[2] is practically crucial for reaching high electric fields and therefore for getting large current densities. Based on our previous results[3] in 2D, we develop here a computational scheme for the case when the field emitter-cathode can be viewed as a periodic array of bumps placed in the centers of a 2D square lattice, while the anode is a flat plane. Figure 1(a) shows a part of the cathode as seen from above the x,y plane with a chosen square—"cell" [vertices's at the origin and at (1,1)]. The view of this cell along the y-axis is shown in Fig. 1(b). The units in Fig. 1 as well as in all our equations are dimensionless, thus, the circle radii and interelectrode maximum distance in physical units R and H, respectively, correspond to $r=1$ and $z=h$. Each individual cathode bump has cylindrical symmetry and its shape is described by a simple function $z=u(r)$, where $r=\sqrt{x^2+y^2}$, such that $u(r)=0$ for $r=1$ and $du/dr=0$ at $r=0$ and $r=1$. In Fig. 1(b), we have set $u(r)=a(1-r^2)^2$, the same as in Ref. 3. This is the form, we shall use in our calculations on this system.

Let $\varphi(x,y,z)$ denote the potential in our system, then $\varphi=0$ at $z=u(r)$ the cathode and $\varphi=1$ for $z=b$ the anode. The problem's symmetry implies that for all $0<z<h$

$$\frac{\partial\varphi}{\partial x}=0 \text{ on the segment } x=1,\ 0<y<1;$$

$$\frac{\partial\varphi}{\partial y}=0 \text{ on the segment } y=1,\ 0<x<1. \tag{1}$$

An approximation (which allows to use the ideas and methods of our previous work[3]) is obtained by noting that the radial derivative of φ should be already very small at $r=1$ and, therefore, we replace (1) by the boundary condition (BC) which is close to it

$$\frac{\partial\varphi}{\partial r}=0 \text{ at } r=1,\ 0<z<h. \tag{2}$$

Replacing Eqs. (1) by (2) hopefully does not introduce a significant error. It makes our problem of computing φ and the current density j in fact 2D. Using this approximation, we are led to the Poisson equation[3,4] in the cylindrical coordinates $0\le r\le 1$, $0\le z\le h$

$$\frac{\partial^2\varphi}{\partial r^2}+\frac{1}{r}\frac{\partial\varphi}{\partial r}+\frac{\partial^2\varphi}{\partial z^2}=\frac{j(r)}{\sqrt{\varphi(r,z)}}, \tag{3}$$

where $\varphi(r,z)$ satisfies Eq. (2) and

$$\varphi[r,u(r)]=0, \quad \varphi(r,h)=1. \tag{4}$$

Equation (3) has such a simple form because of the strong magnetic field, see Ref. 4. For completing the setup, we note that the current density is a function F of the normal component E of the electric field at the cathode

$$j(r)=g(r)F(E), \quad E(r)=g(r)\frac{\partial\varphi}{\partial z}[r,u(r)],$$

$$g=\sqrt{1+\left(\frac{du}{dr}\right)^2} \tag{5}$$

and that the residual part of cathode outside the circles in Fig. 1(a) will give approximately the same current density as the circle boundary at $r=1$. The square root in Eq. (5) comes from (i) taking into account the curvature of the emitter,

[a]Electroic mail: rokhlenk@math.rutgers.edu.

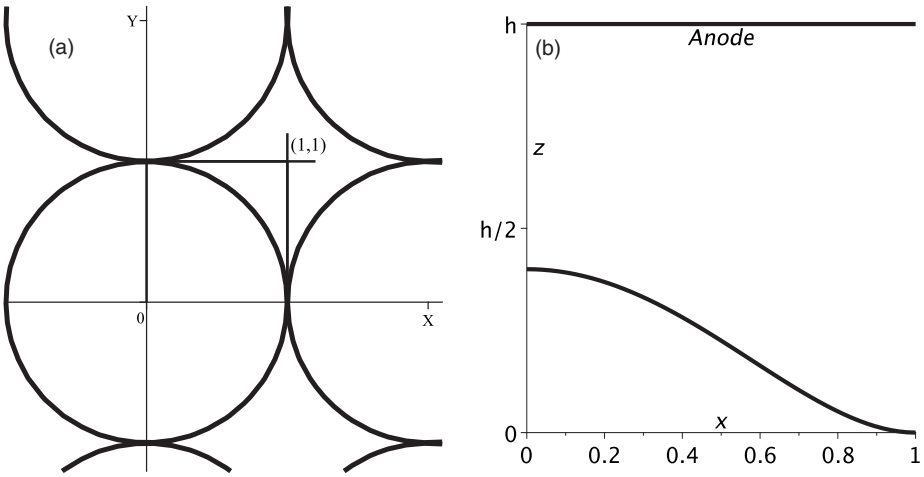

FIG. 1. (a) Schematic diagram of an emitter fraction viewed from above. (b) The "cell" as it is seen along the y-axis.

which increases its area and (ii) converting $\partial\varphi/\partial z$ into the normal derivative.

Assuming that the electric field strength is within the condition of applicability the Fowler–Nordheim–Schottky theory[5] with the Murphi–Good–Forbes corrections[6,7] the current-field law is

$$F(E) = qE^2 \exp(-p/E), \tag{6}$$

where q and p depend on the emitter material and also on E when the field becomes stronger, see below. We use the same numerical quantities here as in Ref. 3 which allows us to obtain results in standard units for the comparison with the 2D computations as well as experiments.

The connection of the above dimensionless quantities, functions, and variables with physical units[8] is the following:

$$\varphi(r,z) = \Phi(X,Y,Z)/V, \quad x = X/R, \quad y = Y/R,$$
$$z = Z/R, \quad h = H/R,$$

$$E(r) = \frac{R}{V}E_n, \quad E_n = |\nabla\Phi|, \quad q = \frac{Q}{\epsilon_o}\sqrt{\frac{mV}{2e}}, \quad p = PR/V,$$

$$Q = 1.54 \times 10^{-6}/t^2(\eta)\chi, \quad P = 6.83 \times 10^7 v_F(\eta)\chi^{3/2},$$
$$\eta = \sqrt{e^3E_n/4\pi\epsilon_o}/\chi,$$

$$t(\eta) = 1 + \eta^2(1 - \ln\,\eta)/9, \quad v_F(\eta) = 1 - \eta^2(1 + \ln\,\eta^{-1/3}),$$

where $\Phi(X,Y,Z)$ is the potential in dimensional variables, V—anode voltage, E_n—electric field strength at the cathode, m and e—electron mass and charge, ϵ_o—electric constant, χ is the electron work function, and numerical values for Q, P assume that χ is taken in electron-volts (more details in[3,7,6]).

II. MODELING THE POTENTIAL

Using the approximation described above, we have to model the potential $\varphi(r,z)$ inside the cylinder $0 \le r \le 1$, $0 \le z \le h$ with high precision in order to get a reliable $j(r)$. We look for a solution of Eq. (3) in the form

$$\varphi(r,z) = \varphi_0(r,z) + \sum_{i=1}^{N-2} c_{i+2}\varphi_i(r,z). \tag{7}$$

In the same way as in Ref. 3 the principal component $\varphi_0(r,z)$ of the potential is modeled as a solution of an algebraic equation

$$z = (1 - \varphi_0)(1 - c_1\varphi_0)u(r) + \varphi_0[h - c_2(1 - \varphi_0)]. \tag{8}$$

The solution φ_0 of Eq. (8) has two free adjustable parameters c_1 and c_2. It satisfies Eq. (4) giving $\varphi_0 = 0$ when $z = u(r)$ and $\varphi_0 = 1$ when $z = h$ as it should, while for intermediate voltages of φ_0 the surface $z(r)$ describes a smooth transition from $u(r)$ to h. Thus Eq. (8) seems intuitively a promising approximation for the equipotential surfaces.

In Eq. (7) φ_0 is supplemented with a set of additional functions φ_i each with an adjustable multiplier-parameter and for them and their derivatives the homogeneous BC must hold. The whole set of these trial functions should help to satisfy Eq. (3) where j is evaluated by Eq. (5) via the normal derivative of φ at the emitter surface $z = u(r)$. We choose the trial functions in the following way:

$$\varphi_1 = g_{3/2} - g_{k+1}, \quad \varphi_l = g_l - g_{k+1}, \quad l = 2,3,\ldots,k;$$
$$k < N, \quad g_l(r,z) = \left[\frac{z - u(r)}{h - u(r)}\right]^l. \tag{9}$$

The function φ_1 plays a special role because its divergent second derivative behaves as $1/\sqrt{z - u(r)}$ when $z \to u(r)$ near the cathode surface similarly to $j/\sqrt{\varphi_0}$. Also, we used the functions $f_m = [z - u(r)]^2(h - z)^2 r^{m+1}$, $m = 1,2,\ldots,n+1$ and $v_i = [z - u(r)](h - z)z^i$, $i = 1,2,\ldots$ for constructing the additional terms

$$\varphi_{m+k}(r,z) = (n+2)f_m - (m+1)f_{n+1}, \quad n < N - 2 - k;$$
$$\varphi_{n+k+i}(r,z) = v_i, \quad i = 1,2,\ldots,N - 2 - k - n. \tag{10}$$

It is easy to see that all these functions satisfy the homogeneous BC. The maximum number N of adjustable parameters never exceeded 20 in our computations. Note that all the parameters c enter in Eq. (3) nonlinearly due to the term $\sqrt{\varphi}$ but c_k for $3 \le k \le N$ are also present in a linear way via the Laplacian in the left side of Eq. (3) which is very sensi-

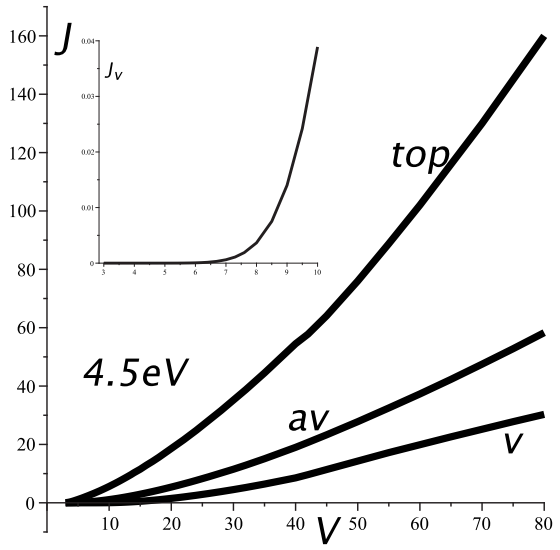

FIG. 2. Top, average, and valley (see insert) current densities vs anode voltage. The emitter parameters are $R=H=1$ μm, $a=0.3$; $\chi=4.5$ eV; V in kV, J in 10^8 A/cm^2.

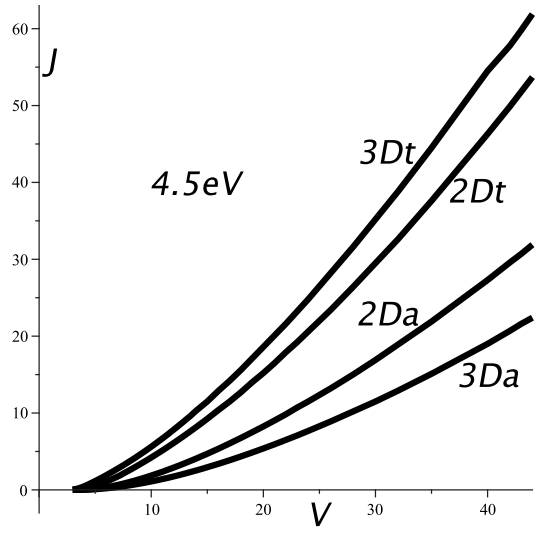

FIG. 3. Top (2Dt and 3Dt) and average (2Da and 3Da) current densities for the 2D and 3D emitters.

tive to them. The contribution to $E(r)$ and, therefore, to the cathode current, see Eqs. (5), (9), and (10), comes from φ_0 and also from φ_l, $l>n+k$ with their c-factors.

III. SOLUTION

Using only the algebraic functions Eqs. (7)–(10) allows us to construct a fast and effective computation procedure. First, a representative set (about a 1000) of discrete points is chosen in the domain $0<r<1$, $u(r)<z<h$ and in each of them the trial solution Eq. (7) is substituted into Eqs. (3) and (5). Then, we identify all the terms linearly dependent on the c's and temporarily neglect the c-dependence of all other terms, collect all in the left side of Eq. (3), square the result and sum up these squares. This sum is minimized by a standard way in terms of c-parameters which come linearly in Eq. (3) and then they will be used in the nonlinear terms on the next step of iteration. As a criteria of the computational accuracy, we require that the functional be minimized. We also try to minimize the z-dependence of the current density, defined as $j=\sqrt{\varphi}\Delta\varphi$, for each r in the whole region, namely, at all the representative points. The number of iterations is always below one hundred, the average current density variations are within 20%, though these variations can be higher for $r\to 1$, where the current density is small and almost does not contribute to the total current.

IV. RESULTS AND COMPARISON WITH 2D EMITTER

As mentioned earlier we use the same parameters as in the 2D system[3] where the cathode consists of a periodic set of parallel ridges whose cross section is the same as in the present bumps. We also use the same work function $\chi=4.5$ eV. Figure 2 shows plots of current densities from the bump top where $r=0$, the valley between two neighboring bumps (v) where $r=1$, and the average current density which can be considered as the total current in our setup (since the total area is 1).

The current pattern is similar to the 2D case though the dominance of the current contribution from the top of the bump is larger. For the same parameters as in Fig. 2, we compare in Fig. 3 the current densities from the bump tops and from the top of the ridges (case of the 2D emitter) as well as the total currents for these cases.

One can see that the 2D emitter produces a larger total current in spite of a lower current density from the tops of the ridges. Nevertheless at low voltages, when the current can be emitted only by the most curved part of the cathode surface, the 3D emitters have some advantage. This is illustrated by Fig. 4, where we show for $a=0.3$ and $a=0.6$ the ratios of 2D over 3D current densities at the top of bumps and similar ratios of the total currents.

Though the emission from the top of separate bumps exceeds the emission from the top of ridges (even more than twice for $a=0.6$ and $V>2.5$ kV when the space charge screening already plays a role) the average and total current from the 3D emitter is larger only when V is "small:" $V<3.4$ and 1.8 kV for $a=0.3$ and 0.6, respectively, in our conditions. Clearly, this effect is stronger when the curvature of cathode bumps is larger as one can see in Fig. 4. The 2D top current density is always smaller than the corresponding 3D density for the same bump height and the same voltage, by factors 8 and 20 in the cases $a=0.3$, $V=3$ kV and $a=0.6$, $V=1.5$ kV, respectively. Note that studying the fields which are not strong enough one might get the wrong impression that the bumps are always better emitters than ridges.

The behavior of the current densities as functions of the individual bump shape are shown in Fig. 5, where the height a of the bump changes from zero to 80% of the maximum distance between the electrodes. The average current density is much lower than the top one which is understandable when a is large but both of them are quite small for the given value of V when $a\sim 0$. Note that the top current density increases not only because of large curvature of the emitter but also due to decreased interelectrode spacing. In Fig. 6,

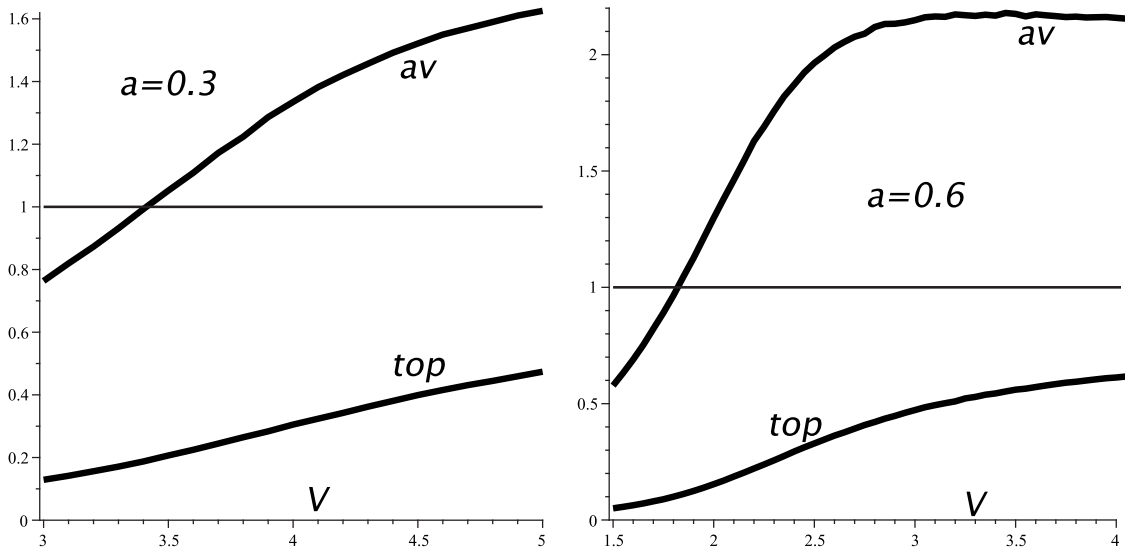

FIG. 4. 2D currents divided by their 3D counterparts for $a=0.3$ and $a=0.6$ The voltage is in kV, $R=H=1$ micron.

we show the same current densities but normalized by the local Child–Langmuir current,[9] i.e., $\epsilon_0\sqrt{2em^{-1}}V^{3/2}L^{-2}(x)$, where $L(x)=H[1-u(x)]$.

The tops of cathode bumps emit a higher current density than the one-dimensional (1D) (i.e., produced by a flat emitter) CL limit even when $V\sim 8$ kV according to our computations which for $a>0.5$ are not very precise (this explains some small irregularities in our plots). The valley current becomes negligible in our setup when $a>0.2$.

The current densities above the CL limit at the bump tops produce a very dense space charge which reduces the electric field[10] at the top and its neighborhood. Consequently, the emission dependence on the bump curvature becomes weaker, see Fig. 6, and thus probably the emitters with sharp spikes (instead of our smooth bumps) would not be more efficient in strong electric fields.

We show in Fig. 7 the top 3D and 2D current densities normalized by the 1D Fowler–Nordheim emission, (see Ref. 11), in the same condition, i.e., the same voltage 8 kV and interelectrode distance $H[1-u(0)]$.

The top current densities are determined by the electric fields there and they are stronger in the 3D case for which the cathode curvature is twice that of one of the ridges (2D). The ratio of currents in Fig. 7 is smaller than might be expected from considerations of electrostatics in the absence of currents due to the space charge screening which becomes more significant when a increases: the emitter comes closer to the anode and the current grows, see Fig. 5.

V. SINGLE BUMP FIELD EMISSION

To gain an understanding the effects of the interaction between bumps, we consider here emission by a single bump whose shape is very close to the one, $u(r)=a(1-r^2)^2$, considered before.

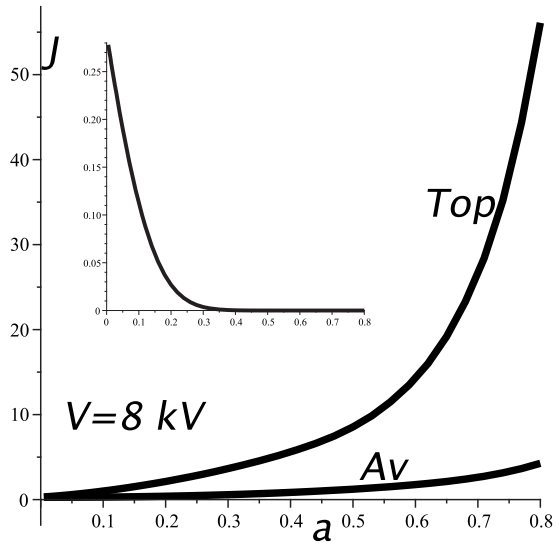

FIG. 5. Plot of current density (A/cm^2) vs the cathode bump height a. Curves (Top) and (Av) represent top and average currents respectively. Inset shows valley current density.

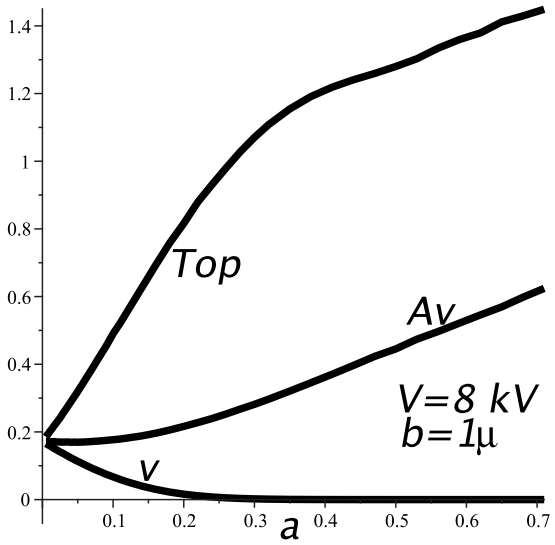

FIG. 6. Top, average, and valley (v) current densities measured in local CL units.

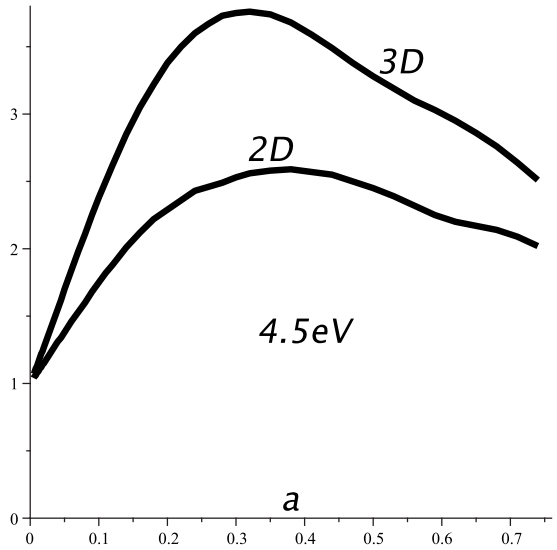

FIG. 7. Top 3D and 2D current densities normalized by 1D emission from flat cathode, $V=8$ kV.

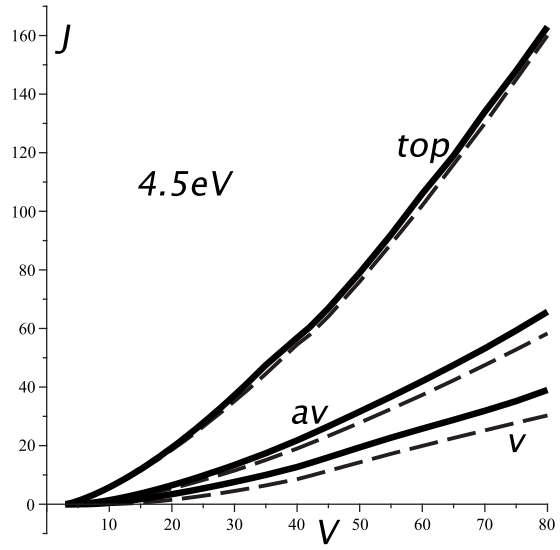

FIG. 8. Top, average, and valley current densities vs anode voltage The dotted lines correspond to Fig. 2.

Our mathematical technique developed for the multi-bump system above uses the function $u(r)$ for modeling not only the bump shape but for also the potential field in all trial functions $\varphi_i(r,z)$, see Eqs. (7)–(10). These functions are chosen to approximate the solution of Eq. (3) for a periodic emitter, where $u(r)$ is defined only for $r \leq 1$. For the case of a single bump, where $0 \leq r < \infty$, $u(r)$ should be replaced by an analytic function which decays sharply for large r. Our choice is a new implicitly defined function

$$u = a \exp[-b(1-u)r^2], \tag{11}$$

with the varying amplitude a as before and an adjustable positive $b(a)$. A preliminary computation shows that for $0.01 < a < 0.6$ the parameter $b(a)$ can be approximated empirically by a linear dependence $b=2.15+2.1a$, it varies from 2.16 up to 3.4 and the bump described by this $u(r)$ has the tip very close to the one used earlier while the overall divergence between the bump shapes reaches 10% only when $r > 0.7-0.8$ where the emission is much lower. This allows us to compare the current from the rectangle in Fig. 1(a) with one quarter of the current emitted by the cathode square $|x| \leq 2, |y| \leq 2$ if the single bump is placed at its center (0,0).

We can keep the trial functions (7)–(9) with the new $u(r)$ which vanishes at $r=\infty$, but instead of functions (10) (which are required to have zero derivatives at $r=1$), we use in this new computation a short set of several functions

$$\varphi_{m+k}(r,z) = (h-z)[y-u(r)][h+z+u(r)]r^2 e^{-qkr^2}, \tag{12}$$

where $q=0.5-1.5$ depending on the value of a. These function provide a flexibility in modeling the Laplacian in Eq. (3) near $z=h$ for different r. The functional to be minimized here involves a larger number of terms because we monitor the computation errors for all $0 < r \sim 10$.

For a fixed $a=0.3$ in Fig. 8, we exhibit the plots of current densities for the single bump together with the corresponding results of the previous section shown in Fig. 2 using the same parameters and units. The single bump produces a somewhat stronger current, the difference is systematic but not significant. The single bump current density marked by "v" will necessarily be larger than its counterpart because the emitter surface there is a little closer to the anode than in the valley. The same can be said about the total current, but in a much smaller measure. This is seen in Fig. 8 where these densities look larger even in absolute units, not only relatively.

Figure 9 compares the average bump current densities in the same setups as functions of the bump height a when $V=8$ kV.

The difference is not large and our comments above can be applied for this case too. The top current emitted by the single bump is also slightly larger in accordance with expectations.

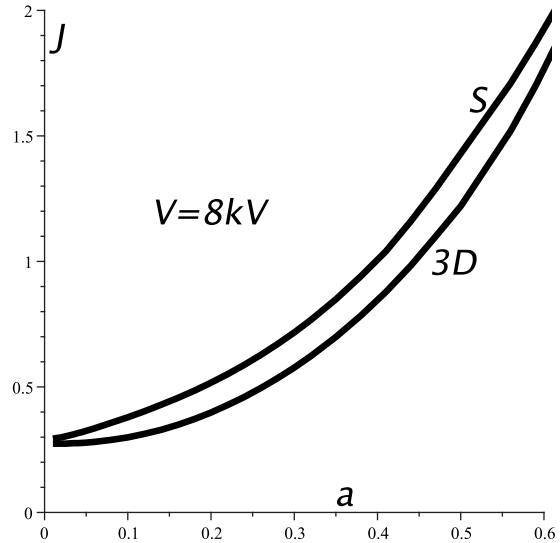

FIG. 9. Plots of average current densities vs bump height for $V=8$ kV. The curves S and 3D correspond, respectively, to the single bump and a bump within a periodic array.

VI. CONCLUSION

We extended our scheme[3] of computation of the field emission for the case of a periodic grid of emitter bumps which have a simple shape and also for the emission by a single bump placed on the flat cathode.

(1) Comparison with the emission from a regular set of parallel ridges of the same cross section (2D case) shows that the 3D emitters give a larger current in weak fields and that their total currents are produced mostly by the emission from the tops of the bumps (this can be damaging for them). In stronger electric fields the 2D emitters with long ridges are more effective and probably less subject to erosion and electric breakdowns.

(2) In strong electric fields the most curved parts of emitter bumps produce a current even higher than the 1D Child–Langmuir limit and, therefore, a very dense space charge. An additional increase in the emitter curvature cannot make the current from the bump tops significantly stronger because the space charge screening reduces the field. Thus the shape of emitter bumps may not be very important in strong fields.

(3) Though the single bump emits somewhat larger current than a bump within the array the difference is small.

ACKNOWLEDGMENTS

Useful comments of R. Barker and J. W. Luginsland are appreciated. Research was supported by AFOSR under Grant No. F49620-01-0154.

[1]R. J. Umstattd and J. W. Luginsland, Phys. Rev. Lett. **87**, 145002 (2001).
[2]W. P. Dyke and J. Trolan, Phys. Rev. **89**, 799 (1953); Y. Feng and J. P. Verboncoeur, Phys. Plasmas **12**, 103301 (2005).
[3]A. Rokhlenko and J. L. Lebowitz, J. Appl. Phys. **107**, 103301 (2010).
[4]A. Rokhlenko and J. L. Lebowitz, Phys. Rev. Lett. **91**, 085002 (2003); Phys. Plasmas **11**, 4559 (2004).
[5]R. H. Fowler and L. W. Nordheim, Proc. R. Soc. London, Ser. A **119**, 173 (1928); W. Schottky, Phys. Z. **15**, 872 (1914).
[6]E. L. Murphy and R. H. Good, Phys. Rev. **102**, 1464 (1956); R. G. Forbes, Appl. Phys. Lett. **89**, 113122 (2006).
[7]R. H. Good and E. W. Müller, *Handbuch der Physik* (Springer-Verlag, Berlin, 1956), p. 176.
[8]R. G. Forbes and K. L. Jensen, Ultramicroscopy **89**, 17 (2001); R. G. Forbes, J. Vac. Sci. Technol. B **17**, 526 (1999).
[9]C. D. Child, Phys. Rev. (Series l) **32**, 492 (1911); I. Langmuir, *ibid.* **2**, 450 (1913).
[10]R. G. Forbes, J. Appl. Phys. **104**, 084303 (2008).
[11]A. Rokhlenko, K. L. Jensen, and J. L. Lebowitz, J. Appl. Phys. **107**, 014904 (2010).